

---

**Physics Bachelor Thesis**

---

**Spin and Orbital Hall Torques in Ferrimagnetic  
Heterostructures**

Teodor Parella i Dilmé

Supervised by Dr. Can Onur Avci  
Tutorized by Dr. Carles Navau Ros

- July 2022 call -

---

## **Declaration of Authorship and Word Count**

I, Teodor Parella i Dilmé, declare that this thesis titled "Spin and Orbital Hall Torques in Ferrimagnetic Heterostructures" and the work presented in it is my own. I confirm that this work submitted for assessment is my own and it is expressed in my own words. All direct or indirect sources used are acknowledged as references. The total count of words is 6224 using the tool provided by Microsoft Office Word. There are a total of 7 figures considered as 200 word-equivalent and 3 figures considered as 400 word-equivalent, which makes a total of 8824 words.

Signed:

---

## Acknowledgements

I would like to express my gratitude to you Can, for enabling me this opportunity. Thanks for your dedication, guidance and transmitted enthusiasm throughout the project. Also, I would like to thank the rest of magnepic group including Silvia, Martín, Stefano and Leo, as they all have made this work possible. Thanks Carles for the tutorship and help provided along the way.

This experience would not have been possible neither without CSIC JAE INTRO 2021-2022 call and Barcelona's institute of material sciences (ICMAB), which have enabled me to use their facilities.

*Teo Parella*

---

## Abstract

Spintronics focuses its study on electron's spin and magnetic moment properties. Thanks to the spin-orbit interaction, interconversion of charge and angular momenta currents is possible, enabling magnetisation control through spin-orbit torques in magnetic multilayers. Very recently, oxidised copper has proven strong spin-orbit interaction properties, making this material a potential candidate for spintronic devices. In the present work, we recall fundamental aspects on spintronics theory and methods for magnetisation characterisation in magnetic multilayers. To enable electrical measurements in the experimental part, we develop from scratch an entire probe station able to perform resistance and pulse experiments, including suitable software for controlling it. We prove the setup efficiency by successfully determining a large damping-like spin-orbit torque contribution on a Pt/thulium-iron garnet ferrimagnetic device, and we exploit it to implement magnetisation switching through current pulses. Ultimately, we design, build and optimise a heterostructure for determining spin-orbit interaction properties on partially oxidised copper.

## Contents

<b>1</b>	<b>Introduction and motivation</b>	<b>1</b>
<b>2</b>	<b>Theory</b>	<b>2</b>
2.1	Spintronics fundamentals . . . . .	2
2.1.1	Spin-orbit interaction . . . . .	2
2.1.2	Spin Hall effect . . . . .	2
2.1.3	Orbital Hall effect . . . . .	4
2.1.4	Spin Hall magnetoresistance . . . . .	4
2.1.5	Ordinary and anomalous Hall effects . . . . .	5
2.2	Current-induced torques in magnetic heterostructures . . . . .	5
<b>3</b>	<b>Measurement methods</b>	<b>7</b>
3.1	Electrical measurements . . . . .	7
3.2	Optical measurements: magneto-optic Kerr effect . . . . .	8
<b>4</b>	<b>Results and discussion</b>	<b>9</b>
4.1	Construction of a probe station for electrical measurements . . . . .	9
4.2	TmIG/Pt bilayer . . . . .	11
4.2.1	Damping-like spin-orbit torque characterisation . . . . .	11
4.2.2	Magnetisation switching through current pulses . . . . .	13
4.3	TbCo/Cu/GdOx/Pt heterostructures . . . . .	14
4.3.1	TbCo layer optimisation . . . . .	14
4.3.2	Device fabrication . . . . .	15
<b>5</b>	<b>Conclusions and outlook</b>	<b>16</b>
<b>6</b>	<b>List of abbreviations</b>	<b>17</b>
<b>7</b>	<b>References</b>	<b>18</b>

## 1 Introduction and motivation

Spintronics field focuses its study on electron's spin, orbital angular momenta and magnetic moment properties. In a broad sense it enables current transport with angular momenta as an additional degree of freedom, finding practical applications in condensed matter physics, data transmission or data storage. Most importantly, spintronics becomes a powerful tool to understand a material's magnetisation, underlying dynamics and manipulation, as it approaches the problem with the study of in-bulk angular momenta. Magnetic torques are the driving phenomena of magnetisation dynamics, and they are the key ingredient to control a material's magnetisation state. A popular available method is the spin transfer torque (STT), where a conducting ferromagnet (FM) magnetisation is driven by an absorbed spin-polarised current. Nevertheless, spin-orbit interaction (SOI) enables interconversion between charge currents and overall angular momenta flow, resulting in the current-induced spin-orbit torque (SOT) phenomena in magnetic multilayers. Enhanced efficiency and properties arise with current-induced SOTs, which makes them a vibrant research area [1].

In the present work, we will first become familiar with fundamental theory on magnetic materials and spintronics [2]. We will develop a theoretical understanding on how spin and orbital angular momenta current can be generated in a material's bulk/interface, and how it may be exploited in magnetic multilayers. Overall, we want to see how SOTs arise and have an effect on the magnetisation. We will also overview basic concepts on measurement methods that may be executed along the thesis. Due to experimental availability, these will probably be electrical characterisation and magneto-optic Kerr effect (MOKE).

Recently, partially oxidised copper has proven strong SOI properties, hence being a potential candidate for spintronic magnetic multilayers [3, 4]. An experiment on a sample able to tune copper oxidation wants to be undertaken in order to study SOI dependency on copper oxide stoichiometry. Therefore we aim to:

- Construct first an entire probe station setup for performing electrical characterisations. Additionally to hardware, convenient software wants to be provided to enable automated resistance measurements and possible magnetisation-switching experiments.
- Evaluate the efficiency on the constructed probe station by characterising the damping-like (DL) SOT of a prefabricated ferrimagnetic thulium iron garnet (TmIG)/ platinum device [5, 6]. If extracted torque magnitude results high and comparable to the expected by the bibliography, magnetisation switching through current pulses will be attempted on the constructed setup.
- Design, construct and optimise samples that enable SOTs electrical characterisation with tunable copper oxide stoichiometry.
- Perform SOTs characterisation on built devices to quantify their dependency on the copper layer oxidation state.

## 2 Theory

### 2.1 Spintronics fundamentals

In solids, angular momenta is present in form of local momenta, lattice dynamics or phonon form. In spintronics, electrons interchange spin and orbital angular momenta (entangled by spin-orbit coupling) with the lattice, through an exchange interaction and crystal field potential. This makes rich angular momenta conversion in the material, and mechanisms exposed in this section may be exploited to generate overall angular momenta flow affecting macroscopic magnetisation dynamics.

#### 2.1.1 Spin-orbit interaction

An important phenomena in spintronics and solid state physics is the SOI, a relativistic effect regarding the interaction of a non-zero spin particle with an electric potential  $V(\mathbf{r})$  [7]. An electron following Fermi-Dirac statistics holds a quantised spin angular momentum  $\mathbf{S}$ , but also orbital angular momentum  $\mathbf{L}$  and total angular momentum  $\mathbf{J} = \mathbf{L} + \mathbf{S}$  in a many-body problem. Magnetic moment arises both from spin  $\mu_S = -g_S\mu_B \frac{\mathbf{S}}{\hbar}$  and angular momentum  $\mu_L = -g_L\mu_B \frac{\mathbf{L}}{\hbar}$ , resulting in an electron's total magnetic moment  $\mu_J = -g_J\mu_B \frac{\mathbf{J}}{\hbar}$  ( $g$  are the Landé g-factors, and  $\mu_B$  Bohr's magneton). Overall, when the electron experiences a magnetic field, it will interact energetically with it according to  $\Delta\mathbf{H} = -\mu_J \cdot \mathbf{B}$ . Considering now the electric and magnetic fields at the lattice reference frame ( $\mathbf{E}, \mathbf{B}$ ), and the corresponding fields at an electron's reference frame ( $\mathbf{E}', \mathbf{B}'$ ) moving through the lattice at speed  $\mathbf{v}$ , the connection between the frames is given by the Lorentz transformations:

$$\mathbf{E}'_{||} = \mathbf{E}_{||} \quad , \quad (1)$$

$$\mathbf{B}'_{||} = \mathbf{B}_{||} \quad , \quad (2)$$

$$\mathbf{E}'_{\perp} = \gamma(\mathbf{E}_{\perp} + \mathbf{v} \times \mathbf{B}) \quad , \quad (3)$$

$$\mathbf{B}'_{\perp} = \gamma(\mathbf{B}_{\perp} - \frac{1}{c^2}\mathbf{v} \times \mathbf{E}) \quad . \quad (4)$$

With  $\gamma = (1 - v^2/c^2)^{-\frac{1}{2}}$  the Lorentz factor. In particular, equation 4 implies the electron experiencing an additional  $\perp$  magnetic field component in its reference frame when an electric field  $\mathbf{E}$  contribution perpendicular to the electron's velocity  $\mathbf{v}$  exists in the lattice frame. Electron's total magnetic moment will interact with the experienced magnetic field, aligning antiparallel to it. This is perceived as the SOI at the lattice reference frame, arising interesting phenomena such as orbital Hall effect, spin Hall effect (SHE) or anomalous Hall effect (AHE) as will be seen in the upcoming sections.

#### 2.1.2 Spin Hall effect

A spin-dependent deviation of an electron's trajectory arises with the SHE, one of the protagonist phenomena in spin-orbitronics. In high SOI materials such as Pt and other heavy metals (HM), when applying a charge current  $\mathbf{j}_c$  electrons with spin orientation  $\mathbf{S}$  are deviated selectively, generating a spin current. This is captured by the spin current tensor  $\mathcal{J}_s$ , which components  $\mathcal{J}_s^{i,j} = \mathbf{j}_{s,i}^j$  represent a local spin component flux polarised in the  $i^{th}$  direction

## 2 THEORY

---

and propagating along  $j^{th}$  direction. An important parameter that captures the conversion efficiency between charge and spin currents is the spin Hall angle  $\alpha_{SHE}$ :

$$\mathbf{j}_s = \alpha_{SHE} \frac{\hbar}{2q_e} (\mathbf{j}_c \times \mathbf{S}) \quad . \quad (5)$$

SHE results in spin-polarised electron accumulation at the material's boundary [Fig.1A]. This angular momenta will be absorbed by contiguous layers and allow the action of SOTs on the magnetisation as will be seen later on.

Two possible mechanisms describing SHE are the extrinsic spin-dependant scattering and the intrinsic contribution [8]. The former is a SOI-based effect that takes place during the multiple scattering processes an electron undergoes in the solid, which can be intuitively understood with the Mott-skew scattering. Electrons interact with a local scattering potential  $V(\mathbf{r})$  (mainly positive nuclei), resulting in a SOI. Considering the electron in rest frame and an approaching scattering potential with oestered field  $\mathbf{H}'$ , the force experienced by the electron follows  $\mathbf{F} = \nabla(S \cdot \mathbf{H}')$ , resulting in an overall spin-dependant scattering direction [Fig.1B]. On top of the Mott-skew scattering, a side-jump effect (relying solely on quantum mechanics) positively contributes on the generated spin current. On the other hand, the SHE intrinsic contribution does not require scattering, but instead relies on band induced mechanisms affecting the spin dynamics of conducting electrons. Present configuration can be described by the Rashba model hamiltonian:

$$H_R = \frac{\hbar^2 k^2}{2m} + \alpha_R (\sigma_x k_y - \sigma_y k_x) \quad (6)$$

With  $\alpha_R$  the Rashba constant. Therefore, an electric field will shift the dynamics of the crystal momenta population  $\mathbf{k}$ , experiencing an effective magnetic field as function of  $\mathbf{k}$  due to SOI [9, 10]. Ultimately, preferential spin population flow emerges as the Fermi surface in the reciprocal space is altered [Fig.2A].

Relying on the same mechanism but in inverted order, the inverse SHE effect does also exist, and may convert a spin current to an electrical one.

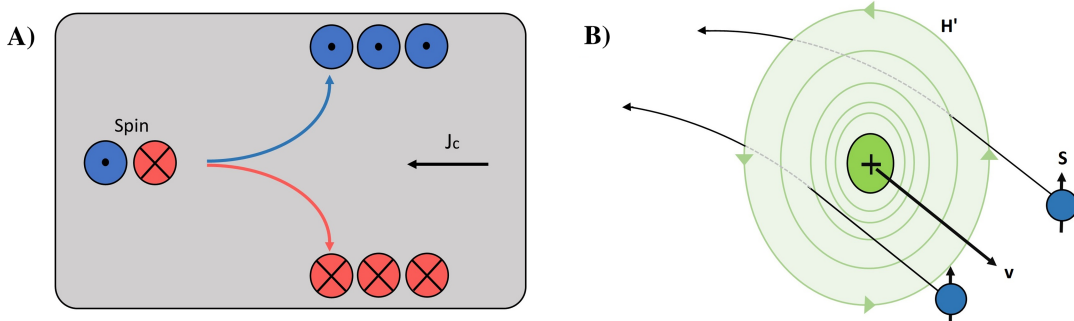


Figure 1: (A) SHE. Spin-dependant deviation of electrons in a HM with charge current density  $\mathbf{j}_c$ . Spins with opposite directions are accumulated at lattice boundaries due to the arising spin current in equation 5. (B) Mott-skew scattering. At the electron's rest frame, if an atom passes on the left side of the electron (velocity  $\mathbf{v}$ ),  $\mathbf{S}$  is parallel to  $\mathbf{H}'$  and it is deviated towards increasing field (left). If the atom passes on the right side of the electron instead,  $\mathbf{S}$  is anti-parallel to  $\mathbf{H}'$  and is deviated to decreasing field (left). Hence, same spin is effectively deviated to the same direction.

### 2.1.3 Orbital Hall effect

On top of spin current, orbital current can be generated in a material's bulk [11]. Analogously as spin population in the reciprocal space is altered in the SHE intrinsic contribution, overall atomic orbitals population are also modified when an E field is applied [Fig.2B]. This does not require inversion symmetry, and generates an angular momenta current which can also be interconverted with spin current through spin-orbit coupling. Ultimately, SHE and orbital Hall effect combined enable angular momenta transmission to a contiguous layer, hence being the trigger of arising SOTs.

### 2.1.4 Spin Hall magnetoresistance

Spin Hall magnetoresistance (SMR) results in a resistivity variation due to the SHE/inverse SHE mechanisms. It is important to highlight that this effect has a strong contribution in FM insulating/ HM bilayers and its magnitude depends on the magnetisation relative orientation. Intuitively, when magnetisation is parallel to spin accumulation, inverse SHE results in charge current generation in the same direction as the applied longitudinal current. However, when contiguous layer absorbs magnetic moment and electrons spin orientation is changed, inverse SHE results in a charge current in the opposite direction. Depending on the relative magnetisation orientation, transversal currents may be also generated in the Y axis, resulting in an easily detected transversal SMR. Overall, SMR will allow to keep track of the magnetisation vector orientation in insulating FM layers through longitudinal/transversal Hall measurements as will be seen in the measurement methods section.

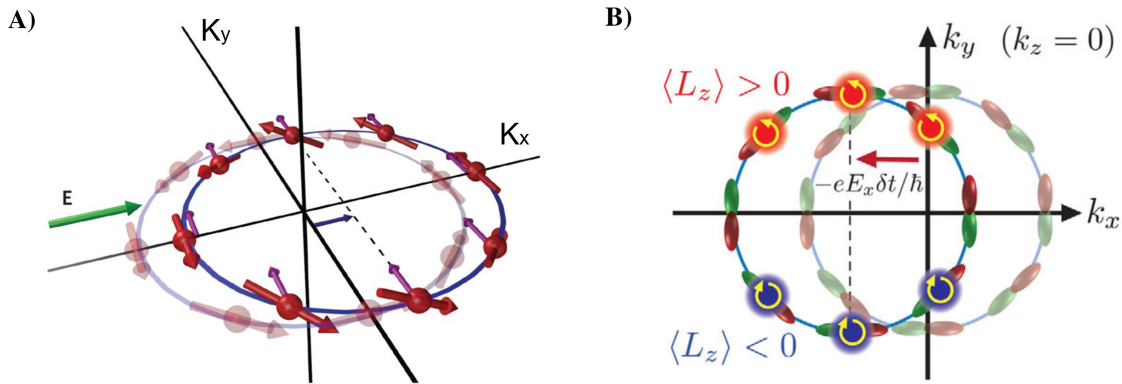


Figure 2: (A) Rashba model visualisation in equation 6 [10]. A Rashba magnetic field is experienced at equilibrium (semitransparent picture). As an electric field is applied, Fermi surface changes as overall momentum (blue arrow) is gained and k-dynamics result altered. An additional  $\mathbf{B}_{eff}$  (pink arrow) is experienced, shifting the Rashba field. Positive momenta in the Y axis will experience an inverted contribution with respect to the negative momenta, resulting in overall spin polarisation and spin current. (B) In analogy to Rashba effect, an orbital texture variation in centrosymmetric crystals takes place when an electric field is applied [11].  $k_y < 0$  states moving in  $-y$  direction gain angular momenta as  $\langle L_z \rangle < 0$ , while  $k_y > 0$  states moving in  $+y$  gain  $\langle L_z \rangle > 0$ . Ultimately, an orbital momenta current is generated perpendicular to the X axis.

### 2.1.5 Ordinary and anomalous Hall effects

Ordinary Hall effect arises when a magnetic transversal field  $\mathbf{B}_\perp$  respect to the current flow  $\mathbf{j}_x = j_o \mathbf{x}$  is present, as charge carriers experience the corresponding magnetic field contribution of the Lorentz force  $\mathbf{F} = q(\mathbf{v} \times \mathbf{B})$ . In particular,  $\mathbf{B} = B_0 \mathbf{z}$  results in effective charge accumulation at the material Y axis boundaries. This is perceived as a Hall resistivity contribution  $\rho_H^{OHE}$  proportional to  $B_0$  along the Y axis.

In FM conducting materials, conducted electrons angular momenta has a preferential value. Relying on the same mechanism as the ordinary Hall effect, additional contributions arise in the form of the AHE. It is important to highlight that it is not the additional contribution of the magnetisation on the overall magnetic field ( $\mathbf{B} = \mu_0(\mathbf{H} + \mathbf{M})$ ), but instead additional SOI spin-dependant processes depending on the magnetisation out of plane (OOP) component, resulting in different charge accumulation:

$$\rho_H = \rho_H^{OHE} + \rho_H^{AHE} = R_H^{OHE} B_0 + R_H^{AHE} M_z \quad . \quad (7)$$

AHE resistivity usually results much larger than the one from ordinary Hall effect ( $\rho_H^{AHE} \gg \rho_H^{OHE}$ ), which is key to perceive magnetisation switching. AHE origins still remain a matter of study, but it is accepted that the same mechanisms contributing to the SHE apply to AHE.

## 2.2 Current-induced torques in magnetic heterostructures

A common approach to manipulate a FM magnetization state with electrical current is by using a STT. By injecting a spin polarised electrical current in a FM, injected electrons will experience an exchange field and start precessing around it in a process called dephasing. Ultimately, electrons align towards the exchange-correlation energy  $\Omega_{xc}$  direction loosing  $\perp$  spin component. Lost angular momenta is transferred to local lattice elements, resulting in a variation on the population's magnetic order. This process modifies the macroscopic magnetisation vector through the STT  $\mathbf{T}_{STT}$ . Therefore, by injecting enough spin polarised current  $j_c$  in a FM, its magnetisation state may be controlled. Nowdays STTs mechanisms find practical applications in random-access memories by manipulating a free layer magnetisation over a fixed magnetisation layer, and allowing memory storage in high/low resistance states. Nevertheless, other approaches improving the energy inefficiency of STT are currently being investigated.

A strong alternative to magnetisation manipulation are SOTs [12]. By passing  $j_c$  through a strong SOI layer next to a magnetic material, spin-orbit angular momentum is accumulated at the interface through SHE and Rashba effect, which may be absorbed by the contiguous magnetic layer. In this case, transferred angular momentum is not only achieved through spin, but also through the interaction of the orbital angular momentum carried by the atomic lattice. Magnetisation dynamics (either with STTs or SOTs) is governed by the Landau-Lifshitz-Gilbert equation:

$$\frac{d\mathbf{m}}{dt} = -\gamma \mathbf{m} \times \mathbf{B}_M + \alpha \mathbf{m} \times \frac{d\mathbf{m}}{dt} + \frac{\gamma}{M_s} \mathbf{T} \quad . \quad (8)$$

$M_s$  stands for the saturation magnetisation, and  $\mathbf{m} = \mathbf{M}/M_s$  magnetisation unit vector. First term of the equation takes into consideration magnetisation precession around an effective

magnetic field  $\mathbf{B}_M = \frac{\delta\mathcal{E}}{\delta\mathbf{M}}$  resulting from the functional derivative of the magnetic energy density  $\mathcal{E}$ . Second term accounts for magnetisation relaxation towards equilibrium position, with  $\alpha$  Gilbert's damping parameter. Third term accounts for remaining torques, which in terms of SOTs can be expressed as

$$\mathbf{T} = \mathbf{T}_{FL} + \mathbf{T}_{DL} = \tau_{FL}\mathbf{m} \times \xi + \tau_{DL}\mathbf{m} \times (\xi \times \mathbf{m}) \quad . \quad (9)$$

That is, as a contribution of a field-like (FL) SOT and a DL SOT.  $\xi$  is a unit vector depending on the microscopic origin of the torques, usually proportional to the direction of spin/angular momenta accumulation orientation. Most importantly, DL (or longitudinal) SOT belongs in the plane defined by  $\mathbf{m}$  and  $\xi$ , and performs magnetisation damping. On the other hand, FL (or transverse) SOT is normal to the mentioned plane, acting on the magnetisation as an effective magnetic field around  $\xi$  axis [Fig. 3]. It has been proven that the DL component is mainly given due to SHE, whilst FL component arises mainly because of Rashba effect. Equivalently, a torque may be expressed as  $\mathbf{T} = \mathbf{M} \times \mathbf{B}_T$ , being  $\mathbf{B}_T$  an associated effective magnetic field on the corresponding torque.

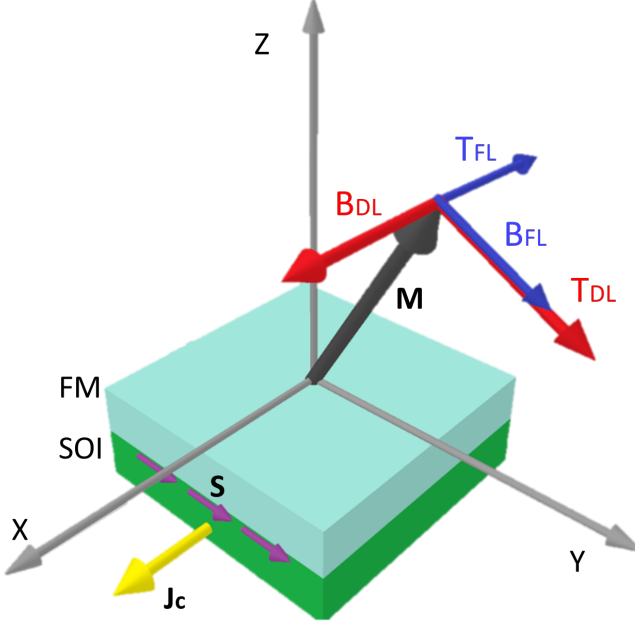


Figure 3: Visualisation of DL and FL SOTs acting on a magnetisation state in the YZ plane. On a bilayer made of a FM in contact with a material with high SOI, while injecting  $j_c$  in the SOI layer, selective spin accumulation  $\mathbf{S}$  takes place at the interface. Spin and overall angular momenta is absorbed in the adjacent FM. In this case  $\xi \propto \mathbf{S}$ , and  $\mathbf{T}_{DL}$ ,  $\mathbf{T}_{FL}$  take their corresponding geometry according to eq. 9.  $\mathbf{M}$  dynamics will follow Landau-Lifshitz-Gilbert equation, with  $\mathbf{T}_{DL}$  having the effect of damping the magnetisation on the  $(\xi, \mathbf{M})$  plane (in this case towards angular momenta injection orientation  $\xi$ ), while  $\mathbf{T}_{FL}$  will rotate the magnetisation vector around  $\xi$  axis.

### 3 Measurement methods

#### 3.1 Electrical measurements

A material's magnetic properties might be characterised through resistivity contributions, obtained with suitable resistivity measurements and an strategically applied external field. From now on, X axis is defined by  $\mathbf{j}_c = j_{c,x}\mathbf{x}$ , Z axis by a positive OOP field direction  $\mathbf{H}_{OOP} = H_0\mathbf{z}$  normal to the sample's surface, and  $\mathbf{y} = \mathbf{z} \times \mathbf{x}$ . Polar and longitudinal angles characterising  $\mathbf{M}$  are defined as  $\theta$  and  $\phi$  respectively. Introducing now the resistivity tensor, which exposes in a general form electrical transport properties of a material by connecting the electric field  $\mathbf{E}$  with the current density  $\mathbf{j}_c$ :

$$\begin{pmatrix} E_x \\ E_y \\ E_z \end{pmatrix} = \begin{pmatrix} \rho_{xx} & \rho_{xy} & \rho_{xz} \\ \rho_{yx} & \rho_{yy} & \rho_{yz} \\ \rho_{zx} & \rho_{zy} & \rho_{zz} \end{pmatrix} \begin{pmatrix} j_{c,x} \\ j_{c,y} \\ j_{c,z} \end{pmatrix} . \quad (10)$$

Diagonal tensor elements are longitudinal resistivities and non-diagonal elements are transversal resistivities manifestation due to longitudinal current (Hall effects). The variation of the resistivity tensor as function of applied external field and magnetisation state is the main object of study in this section. By considering anisotropic magnetoresistance as dominant contribution to SMR (that is, resistivity depends only on  $\mathbf{M}$  and  $\mathbf{j}_c$  relative orientation), longitudinal resistance can be proven to be

$$R_w^L = R^{SMR} \sin^2 \theta \sin^2 \phi , \quad (11)$$

with  $R^{SMR}$  the maximum longitudinal SMR. Hall resistance can be proven to satisfy

$$R_w^H = \frac{V_H}{I} = R_H^{AHE} \cos \theta + R_H^{SMR} \sin^2 \theta \sin(2\phi) + R_H^{OHE} H \cos \theta_H . \quad (12)$$

With  $\theta_H$  the external field polar angle and  $R_{SMR}$ ,  $R_{AHE}$ ,  $R_{OHE}$  the maximum SMR, the SMR-induced AHE resistance and the ordinary Hall effect resistance respectively. Therefore, all mentioned contributions can be determined by saturating the material magnetisation with an external field  $\mathbf{H}$ . Further information can be inferred by considering time-dependant measurements on the samples. In particular, new parameters relying on the magnetisation dynamics (for instance, SOTs) can be calculated. Here, contributions of different harmonics will be exploited as  $V_{total} = \sum_i c_i V^i$ . Measurements may be performed by injecting AC or DC  $\mathbf{j}_c$ , but the former will be considered:

$$V(t) = R(t) I_0 \sin(wt) . \quad (13)$$

Measured resistance may be expressed as function of the magnetic field as

$$R(\mathbf{B}) = R(\mathbf{B}_0 + \mathbf{B}_I(t)) = R(\mathbf{B}_0 + [\mathbf{B}_{FL}(t) + \mathbf{B}_{DL}(t) + \mathbf{B}_{Oe}(t)]) , \quad (14)$$

being  $\mathbf{B}_0$  the sum of external, demagnetising and anisotropy fields, and  $\mathbf{B}_{DL}$ ,  $\mathbf{B}_{FL}$ ,  $\mathbf{B}_{Oe}$  the DL, FL and oestered fields respectively. Expanding  $R(\mathbf{B})$  to first order, a resistance approximation for small  $\mathbf{B}_I$  results

$$R(t) \simeq R(\mathbf{B}_0) + \frac{dR}{dB_I} \mathbf{B}_I \sin(wt) . \quad (15)$$

### 3 MEASUREMENT METHODS

---

Combining 13, 14 and 15 results in

$$V(t) \simeq I_0 \left[ \frac{1}{2} \frac{dR}{d\mathbf{B}_I} \mathbf{B}_I + R(\mathbf{B}_0) \sin(wt) - \frac{1}{2} \frac{dR}{d\mathbf{B}_I} \cos(2wt) \right] \equiv I_0 [R_0 + R_w \sin(wt) + R_{2w} \cos(2wt)] \quad (16)$$

with  $R_0, R_w$  and  $R_{2w}$  the zero, first and second harmonic components, applicable to both transverse/longitudinal directions separately. Note that  $R_w^L, R_w^H$  have been given in equations 11 and 12. Second Hall harmonic reads

$$R_{2w}^H = (R_H^{AHE,SMR} - 2R_H^{SMR} \cos \theta \sin 2\phi) \frac{d \cos \theta}{dH} \frac{H_{FL}}{\sin(\theta_H - \theta)} + 2R_H^{SMR} \sin^2 \theta \cos 2\phi \frac{H_{DL}}{H \sin \theta_H} \quad (17)$$

Second longitudinal harmonic expression could also be derived if needed. Experimentally, transversal voltage will be measured and decomposed into harmonics through a fast Fourier transform to infer the harmonic contributions. This enables DL and FL fields acquisition.

#### 3.2 Optical measurements: magneto-optic Kerr effect

Magneto-optical effects may also be exploited to measure a material's magnetisation state. In particular, in the MOKE a reflected polarised electromagnetic wave enables magnetisation characterisation. Sending a polarised light source  $\mathbf{E}^i = (e_p^i, e_s^i)$  to a material surface ( $p$  indicates incident-plane and  $s$  out of incident-plane) results in a reflected wave

$$\mathbf{E}^{ref.} = \begin{pmatrix} e_p^{ref.} \\ e_s^{ref.} \end{pmatrix} = \begin{pmatrix} r_{ss} & r_{sp} \\ r_{ps} & r_{ss} \end{pmatrix} \begin{pmatrix} e_p^i \\ e_s^i \end{pmatrix} \quad (18)$$

defined by the reflection coefficients  $r$ . On a multilayer, underlying magnetic layers might affect total interface roughness and overlayers properties, hence modifying the surface reflection tensor coefficients. Being  $\epsilon$  the electrical permittivity, polarisation variation results

$$\Delta \mathbf{P} = \epsilon (\mathbf{M} \times \mathbf{E}) \quad . \quad (19)$$

Three main different MOKE experiments might be considered depending on the magnetic layer magnetisation direction. In the case of an OOP sample where  $\mathbf{M} \perp$  to the sample surface, we face a Polar MOKE situation. A linearly polarised light source in the incident plane, results in a  $s$  component gain, whilst linear light source perpendicular to the incident plane, results in a  $p$  component gain. Overall, incident linear polarised light results elliptically polarised after reflection. If the sample is in plane (IP) magnetised, there is longitudinal MOKE if  $\mathbf{M}$  is in the incident plane. In this scenario, polarisation variation of the  $p$  and  $s$  components of incident polarised light results the same as in the OOP magnetisation case. Otherwise, if the IP magnetisation is perpendicular to the incident plane, resulting polarisation results linear in the same direction, but with an intensity variation. In this case, the last linear polarizer in the setup has no effect, but we can still characterise the sample with resulting light intensity.

In the experiments performed in this work, laser light has been initially sent through a linear polarizer and reflected on the sample. Reflected light has been passed again through a linear polarizer to focus only on a single component of the polarised light, which direction has been set to offer maximum resulting intensity at the initial magnetisation state. The light beam intensity has been recorded on a sensor, and the sample has been set on top of a hand-crafted electromagnet with magnetic core.

## 4 Results and discussion

### 4.1 Construction of a probe station for electrical measurements

A probe station able to perform electrical characterisation on magnetic devices has been designed and built from scratch [Fig. 4]. On an optical table, a 3470 GMW electromagnet has been set with the intention of applying IP magnetic fields. In order to apply OOP magnetic fields, a second smaller electromagnet has been handcrafted from copper coil and incorporated within the space of the big electromagnet. A support has been set at the top of the smaller electromagnet to hold the samples. For controlling electromagnets at will, a National Instruments USB controller has been used to transform digital computer output to two different analog currents. These have been imputed to two different Kepco power supply amplifiers, which signals have been imputed to the electromagnets. Generated magnetic field magnitude is limited by magnets overheating: IP (OOP) magnet achieves a maximum of approximately  $H_x = 1500$  ( $H_z = 150$ )  $Oe$  in continuous mode, but up to  $H_x = 2500$  ( $H_z = 400$ )  $Oe$  if the experiment is carried out fast enough.

Two handcrafted supports have been incorporated next to the magnets, each holding two dynamic conducting tips (four tips in total) used for landing and applying/measuring voltage on the samples. The tips have been connected to a handcrafted switch box with multiple functionalities. On the one hand, the switch box has been connected to a Zurich MLFI lock-in amplifier instrument, allowing both current input and measurement on the samples. On the other hand, the switch box enables the connection of two tips to a multimeter in order to check

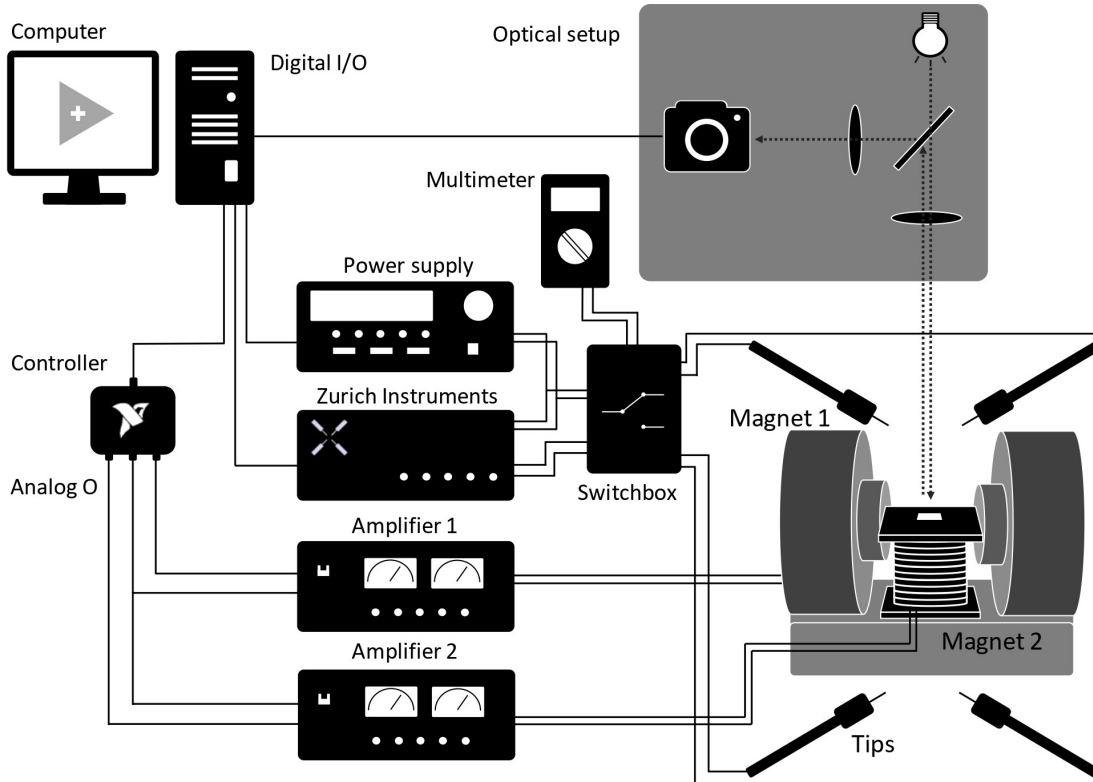


Figure 4: Constructed probe station scheme. An optical setup and a multimeter permits effective tip landing on the devices. The rest of the elements allow automated field scan tasks both IP and OOP.

## 4 RESULTS AND DISCUSSION

---

for effective contact on the samples or perform device resistance measurements. Interchange between lock-in amplifier current input and a Keithley 6221 device is also possible, allowing electrical pulse input for magnetic switching experiments by applying low-amplitude AC current with desired offset. A T-shaped AC current bypass has been included in the middle of the power supply, lock-in amplifier and switch box, to ensure that all the desired current is imputed through the device.

A breadboard has been vertically placed on top of the magnets, holding an optical setup to visualise tip landing on small devices. Such optical setup includes a 20mm focusing lens on the sample, a 50:50 reflecting prism, a light bulb and a second 20mm lens that focuses the resulting image on its focal plane, where a camera is set. Therefore, while preparing an experiment the camera might be used to visualise live tip landings on the devices together with the multimeter in resistance measurement mode until effective contact is provided [Fig.5].

A LabView program controlling the whole setup has been programmed, enabling automated experiments on the devices [Fig.6]. The program allows magnets intensity control and adjustable parameters on the Zurich instruments, such as AC intensity, frequency or harmonic order among others. Automated IP and OOP field sweep scans can also be performed by providing max/min magnetic field, magnetic field step, waiting time between step, measures per step or total number of loops. Plots for IP and OOP field sweeps are continuously updated while undertaking the experiment, allowing data acquisition along the way. On top of this, a

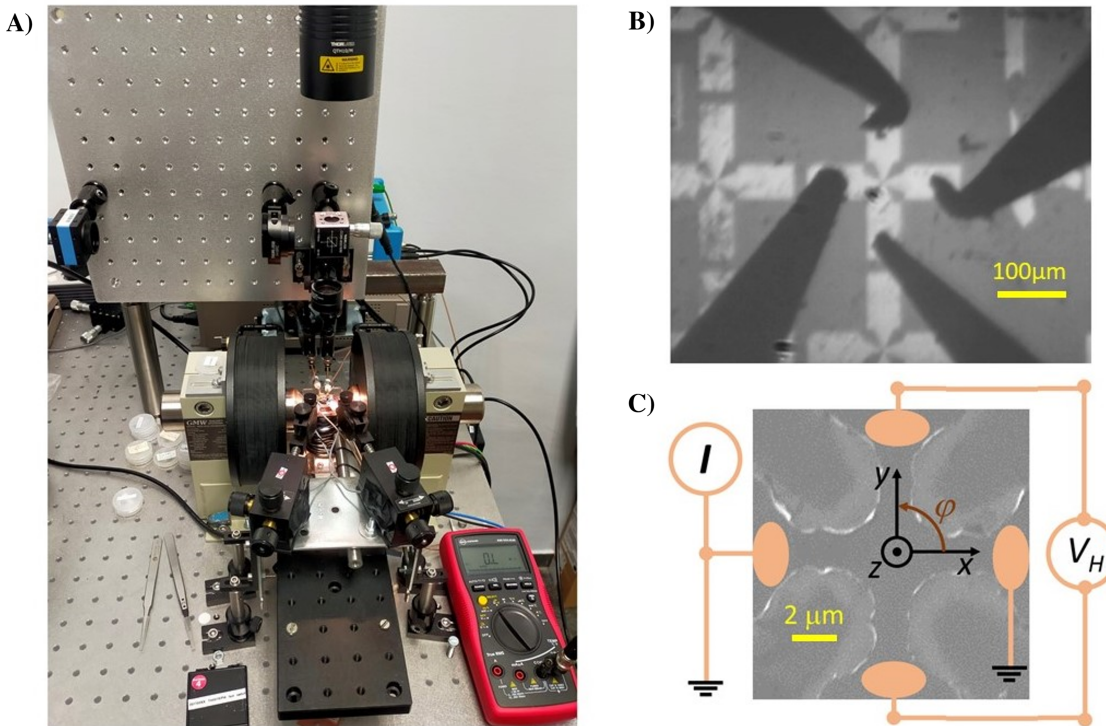


Figure 5: (A) Magnets, tips and optical setup of the constructed probe station. Tips can be manually adjusted to land on the desired zone of the devices. (B) Computer visualisation of landed tips on a device with 4 pads. Two of them allow applying AC on a conducting layer while the other two measure transversal voltage. (C) Visualisation of the central part of the TmIG device under microscope.

## 4 RESULTS AND DISCUSSION

---

second LabView program has been developed to perform switching experiments by enabling iterations of pulse generation and reading. Pulses are generated from the Keithley with desired duration and offset, while a constant magnetic field is applied on the sample. LabView programs are provided at [https://github.com/teoparella/ProbeStation\\_Labview](https://github.com/teoparella/ProbeStation_Labview). Such LabView programs have driver dependencies on the camera, Keithley power supply, NI controller and Zurich lock-in amplifier.

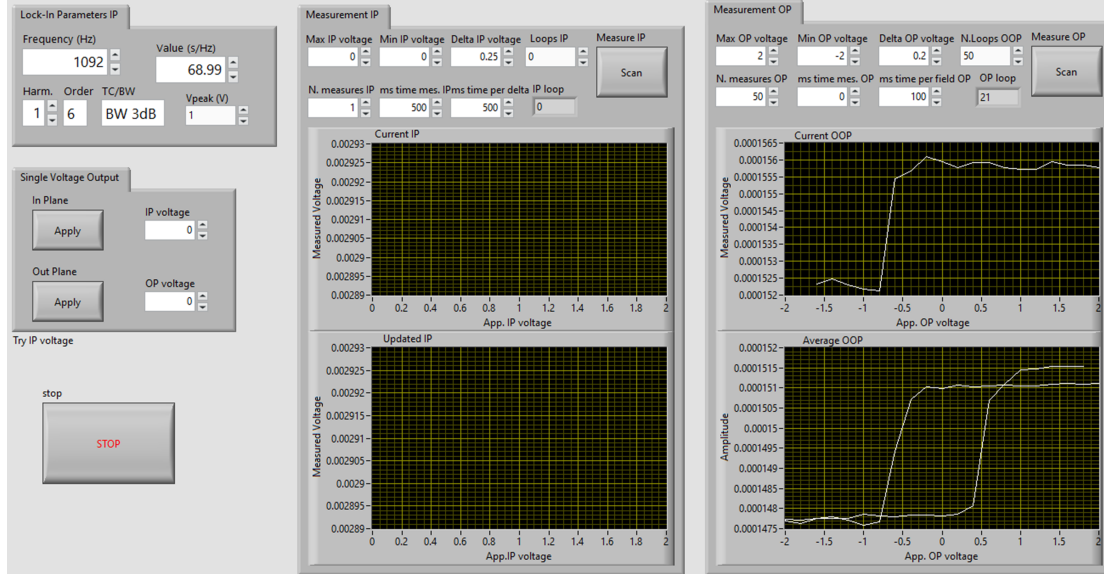


Figure 6: User interface of the LabView program developed and used for magnetic field sweeps. An OOP field scan is currently being undertaken on a OOP magnetised sample over multiple loops, displaying both current loop data (top right) and averaged loops (bottom right).

### 4.2 TmIG/Pt bilayer

The studied sample consists of a  $9.6\text{nm}$  TmIG ferrimagnet ( $3\text{Tm}_2\text{O}_3 \cdot 5\text{Fe}_2\text{O}_3$ ) layer grown on top of a gadolinium gallium garnet (GGG) ( $3\text{Gd}_2\text{O}_3 \cdot 5\text{Fe}_2\text{O}_3$ ) substrate, and a  $4\text{nm}$  Pt layer on top. GGG substrate enables TmIG formation effective, as the crystalline structure of the garnets is the same. Trivalent cations in the garnet forbid electron mobility in the lattice, resulting in high resistivity (insulators). TmIG layer is grown with perpendicular magnetic anisotropy (PMA) and OOP preferential orientation axis.

#### 4.2.1 Damping-like spin-orbit torque characterisation

In order to asses the capacity of the current probe station to undertake electrical measurements, the DL torque of a TmIG has been electrically determined through magnetoresistance characterisation [5]. Such device has a cross-section of  $1.2 \cdot 10^{-14} \text{ m}^2$ , with a measured longitudinal resistance of  $R_l = 1361\Omega$ . Longitudinal AC voltage of  $\langle V \rangle = 4.0\text{V}$  has been applied on the sample in the following experiments with the lock-in amplifier [Fig.5C]. Equivalent current density used results  $\langle J_c \rangle = 2.45 \cdot 10^{11} \text{ Am}^{-2}$ .

Initially an OOP field sweep has been undertaken to appreciate the variation on the first harmonic resistance  $R_w^H$  as function of the magnetisation and extract the AHE contribution.

## 4 RESULTS AND DISCUSSION

---

As the sample is OOP oriented ( $\theta = 0$ ), only AHE and ordinary Hall effect components are appreciated (eq. 12). After voltage harmonic conversion to resistance, the value of  $R_H^{AHE,SMR} = 0.0037280\Omega$  has been extracted, corresponding to the hall resistance variation between up and down magnetisation states [Fig.7A].  $R_H^{OHE}$  has not been needed, but it could be determined on the tails slope of the previous figure by applying high OOP fields.

To extract  $R_H^{SMR}$ , the magnetisation has been moved from OOP configuration by applying IP field scans.  $\phi = 0, \frac{\pi}{4}, \frac{3\pi}{4}$  IP magnetic field orientation has been applied, in order to maximise/minimise the  $\sin(2\phi)$  term in equation 12. The  $\theta$  value on such equation has been modified along the IP field scans (each with fixed  $\phi$ ), until full IP magnetic saturation is achieved at high fields [Fig.7B].  $R_H^{SMR} = 0.022655\Omega$  has been extracted as the resistance difference at  $\phi = \frac{\pi}{4}/\frac{3\pi}{4}$  between OOP and IP magnetisation saturations.

As measured, SMR results much larger than SMR-induced AHE. Here, by making  $R_H^{AHE}$  negligible in front of  $R_H^{SMR}$  and by performing an IP field sweep scan at  $\phi = \pi/4$ , the second harmonic in equation 17 is simplified to

$$R_{2w} = 2R_H^{SMR} \sin^2 \theta \frac{H_{DL}}{H} , \quad (20)$$

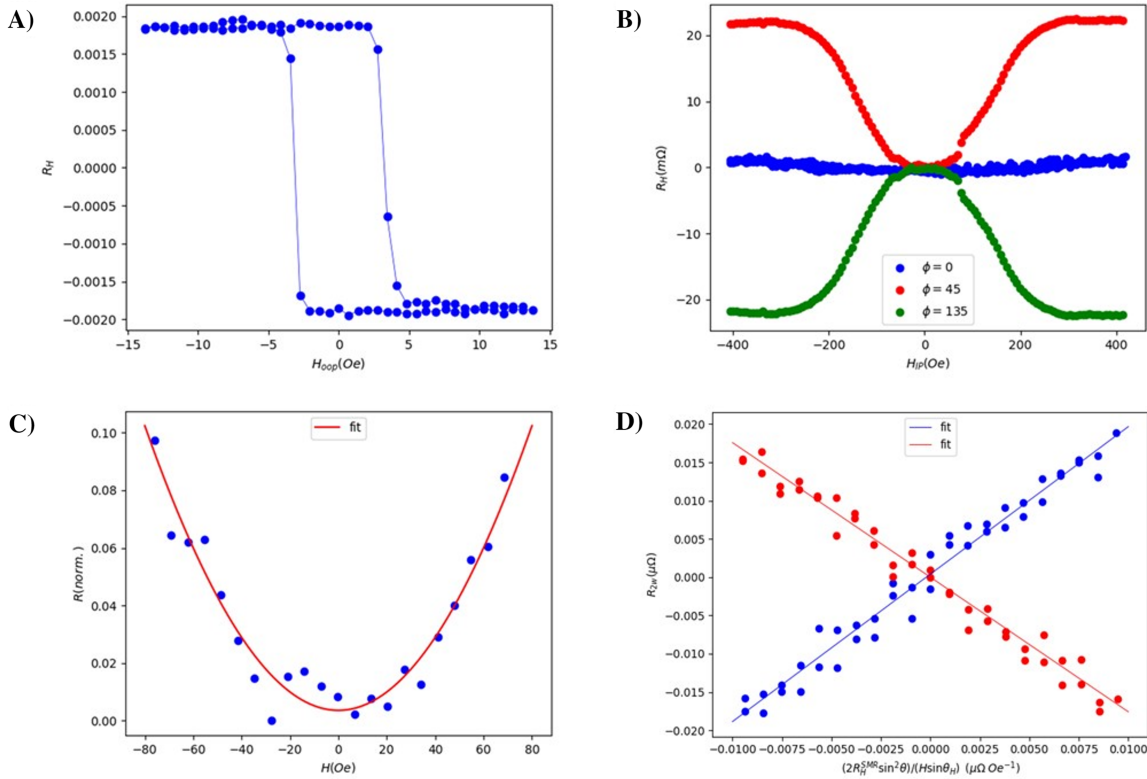


Figure 7: TmIG characterisation. (A) OOP field sweep (B) IP field sweep at  $\phi = \frac{\pi}{4}$ . (C) Sine-squared function fit to normalised  $\phi = \frac{\pi}{4}$  IP sweep. Adjusted R-square = 0.92913. (D) Second harmonic hall resistance as function of calculated  $(2R_H^{SMR} \sin^2 \theta)/(H \sin \theta_H)$ . Linear fit directly extracts the DL-field.

## 4 RESULTS AND DISCUSSION

---

as  $\sin \theta_H = 1$  in a IP scan. Only missing variable is  $\theta$ , which is inferred as function of the IP magnetic field by fitting the sinusoidal-squared function  $R = R_0 + \sin^2(k(H - H_c))$  in figure 7A, following equation 12. Only low fields have been considered, as this is the region where the formulas have been derived. Resulting fitted function has resulted in  $k = 0.0019188 Oe^{-1}$ , extracting the dependency  $\theta = kH$  [Fig. 7C]. Ultimately,  $R_H^{2w}$  has been plotted as function of the variable  $(2R_H^{SMR} \sin^2 \theta)/H$  extracting the DL field  $B_{DL} = 1.843 Oe$  as the average slope on the second harmonic field sweep scan [Fig. 7D]. Results of the DL SOT are about 10 times lower than other similar experiments found in literature [5, 6]. Nevertheless, the DL contribution is relatively large and may be exploited to perform magnetisation switching on the device through current pulses.

### 4.2.2 Magnetisation switching through current pulses

Determined DL SOT has been exploited to switch magnetisation on the TmIG device through electrical pulses in the adjacent Pt layer. By using the *PulseSwitching.vi* developed LabView software, 10ms-long pulses with amplitude offset ranging  $j_{c,x} = \pm 4 \cdot 10^{11} Am^{-2}$  have been sequentially applied in a 20 Oe IP field along the X axis. Results have been averaged over 50 loops, with 150 measures per loop point [Fig. 8]. Frequency on lock-in amplifier ac and Keithley ac+offset pulses is set according to ac bypass threshold in order to provide all generated current on the device. Determined current threshold for magnetisation switching results  $j = \pm 1.458 \cdot 10^{11}$ .

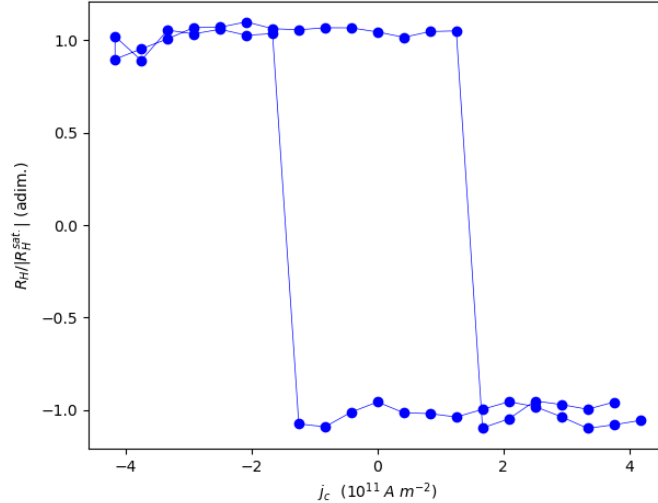


Figure 8: Normalised Hall resistance with respect to the saturation resistance value  $R_H^{sat}$ . of the TmIG device as function of the 10ms current density passing through the Pt layer. A constant 21.6Oe IP field has been applied throughout the experiment. 10 loops of 50 measures per step each have been averaged.

### 4.3 TbCo/Cu/GdOx/Pt heterostructures

Particular interest is given now on copper oxide, as it may be a suitable candidate for the generation of spin currents in multilayers given recently reported SOI properties [3, 4]. Here, we design a bilayer consisting of a FM as magnetic layer in contact to a tunable partially oxidised Cu layer. On the one hand, we select terbium cobalt as conducting ferrimagnet to allow simplified signal acquisition due to its large AHE contribution. Furthermore, PMA has been reported in thin films if the sample stoichiometry is optimised [13]. On the other hand Cu oxidation is attempted by introducing an oxide layer on top of the Cu, and a final Pt layer covered on top to apply electrical gating between Pt and Cu layers. Dielectric Gadolinium oxide has been selected as oxide layer due to previously reported oxygen diffusion with electrical gating [14]. Selected layers widths are exposed in [Fig.10A].

#### 4.3.1 TbCo layer optimisation

We focus now in the TbCo/CuOx bilayer involved in the final device. The TbCo ferrimagnetic layer PMA has to be optimised with OOP preferential orientation axis, ideally with low coercivity considering that the current magnet implemented in the probe station is not able to sustain fields larger than  $\pm 400\text{Oe}$ . In this case, multiple Pt 10nm on top of TbCo 8nm on top of Ti 3nm thick layers have been deposited through DC-magnetron sputtering on GGG as continuous films, with varying stoichiometry on the  $\text{Tb}_x\text{CO}_{(1-x)}$  layer. Samples have been analysed using MOKE in order to infer layer magnetisation properties as function of its composition [Fig. 9].

An IP to OOP magnetisation transition is observed when switching from  $x = 0.20$  to  $x = 0.25$  stoichiometries. For  $x = 0.24$ , the coercive field is low enough while preserving clear OOP magnetisation anisotropy, making this stoichiometry a suitable one for building the devices. Samples coercivity might be subject to mild variations when shaped by photolithography.

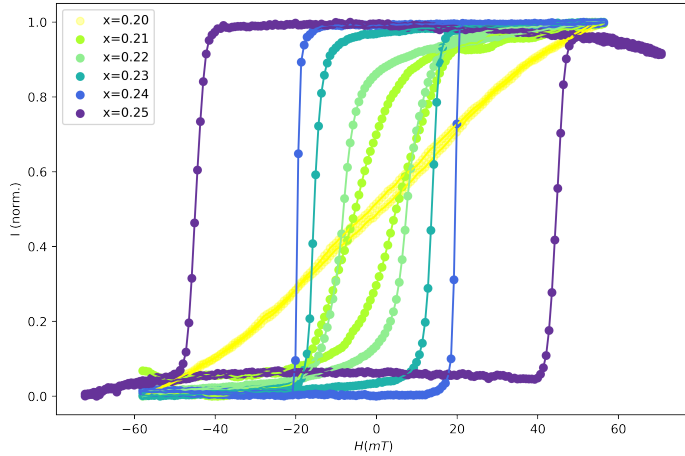


Figure 9: Pt 10nm on top of  $\text{Tb}_x\text{CO}_{(1-x)}$  8nm on top of Ti 3nm thick continuous films. Normalised MOKE intensity as function of applied OOP magnetic field on TbCo stoichiometries ranging  $x = 0.20 - 0.25$ .

## 4 RESULTS AND DISCUSSION

---

### 4.3.2 Device fabrication

Device shapes have been designed with large contact pads in order to simplify the tip landing action on the probe station. An oxidised silicon wafer has been prepared with photolithography, with the desired devices shapes.

Materials have been deposited through DC-magnetron sputtering. In a  $3mTorr$  argon atmosphere, an initial  $3nm$  thick titanium layer has been added as a buffer (or addition) layer, which ensures good cohesion and crystalline transition between the silicon substrate and upcoming layers. On top, a  $8nm$  thick TbCo layer has been sputtered with variable desired stoichiometry ( $x = 0.21$  and  $x = 0.24$ ), and a  $4nm$  copper layer has followed it. Finally a thin  $2nm$  gadolinium layer has been added to prevent Cu oxidation. A second sputtering step has involved changing the sample from the neutral atmosphere chamber to the oxygen chamber, allowing an oxygen-saturated atmosphere to grow the oxide on top. Further Gd has been slowly deposited over 1 hour to allow an overall formation of a  $25nm$  layer. A second photolithography step has been undertaken to place the  $10nm$  Pt gating contact layer on top, with the corresponding pads [Fig.10]. All sputtering guns have been previously calibrated. Desired stoichiometry and width on the final  $8nm$  TbCo layer has been accomplished by varying Tb/Co guns power and sputtering time accordingly.

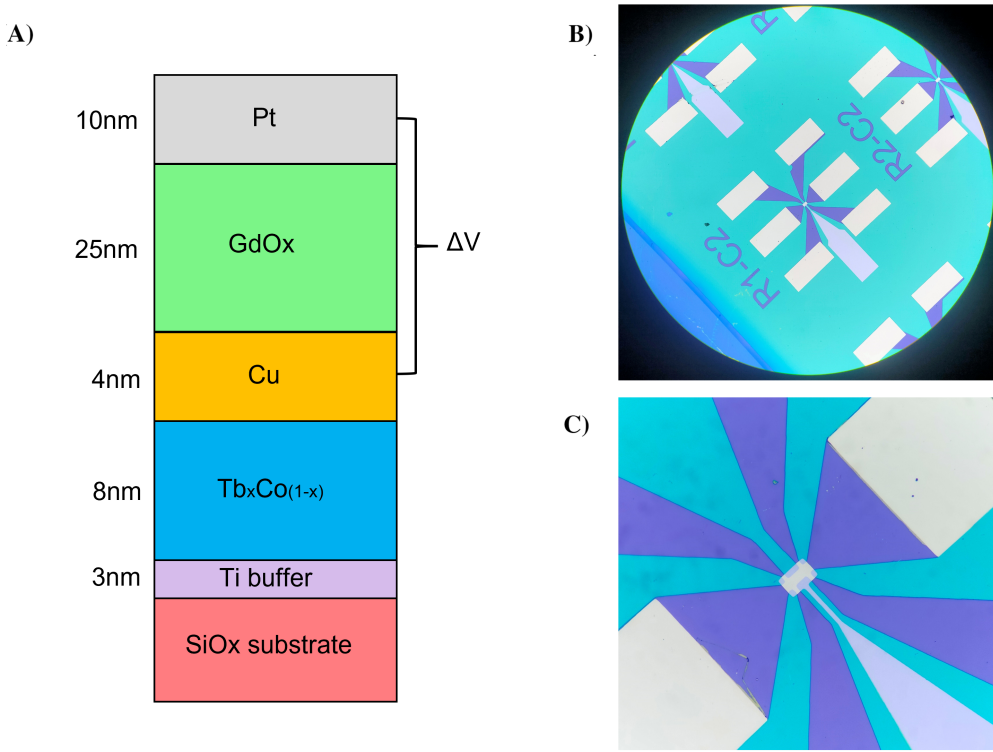


Figure 10: Constructed TbCo/Cu/GdOx/Pt heterostructure. (A) Grown layers order and thickness. Electrical gating between Pt and Cu layers will enable oxygen pump and partially oxidise the Cu layer. (B) Final devices seen under microscope. Each consists on six white pads connected to the TbCo/Cu layers for imputing/measuring voltage on the sample, and a grey pad connected to the Pt layer enabling electrical gating. (C) Zoom in the central part of the device. The last pad (grey) has been shaped and deposited on top of the rest after performing a second photolithography step.

## 5 Conclusions and outlook

In this thesis theory on the main effects present in thin bilayers consisting of a HM with high SOI in contact with a FM have been reviewed. SOI phenomena has proven to arise a large spectrum of effects involving spin and orbital currents that might be exploited in advantage in magnetic multilayers. Spin-orbital angular momenta flow and arising FL and DL SOTs have proven to be efficient tools to influence the magnetic layer magnetisation dynamics. MOKE and magnetoresistance measurements have been exposed as suitable and available methods for magnetisation characterisation.

An entire probe station setup performing magnetoresistance measurements has been constructed from scratch, enabling increased versatility with respect other setups. Complete software has been coded and provided, enabling both convenient automatised magnetoresistance measurements and magnetisation switching experiments through current pulses. Although the setup has proven to be self-sufficient, additional user-friendly improvements on it could be made in the future. On the one hand, a unique computer with preinstalled drivers should be implemented. Additionally, a second monitor could be included over the optical setup, showing the camera vision and helping the user during the tip landing process on the samples. OOP handcrafted magnet might be a magnetic field threshold for experiments requiring  $H_z > 400Oe$ , so a magnet with a larger core could also be implemented.

Constructed probe station has successfully characterised a Pt/TmIG ferromagnetic device. In particular, first harmonics in a OOP and IP magnetisation sweep scans and a second harmonic IP field sweep scan, have enabled to extract the DL SOT field value. The large DL SOT contribution of  $1.843Oe / 2.45 \cdot 10^{11} Am^{-2}$  has been used to perform a magnetisation switching experiment with current pulses. Effective magnetisation control has also proven to be possible with the current setup and TmIG sample, with a determined  $10ms$  current pulse threshold of  $j = \pm 1.458 \cdot 10^{11}$  when a constant IP field of  $H_{IP} = 21.6Oe$  has been applied. Additional implementations could be included in the pulse experiments software, for instance a constant amplitude pulse experiment with varying IP magnetic field.

Finally, material layers have been learnt to be deposited on a substrate using DC sputtering. The design of a heterostructure consisting of TbCo ferrimagnet layer, Cu and gadolinium oxide/Pt gating layers on top has been carried out successfully. The magnetic layer stoichiometry has achieved optimised PMA with OOP preferential axis. IP to OOP preferential magnetisation axis transition has been detected in the range within  $x = 0.20 - 0.25$  on the  $Tb_xCo_{(1-x)}$  stoichiometry.  $x = 0.24$  has ultimately been considered as a suitable stoichiometry to be used in the sample, as OOP orientation has been clearly retained while possessing relatively low coercivity at the same time ( $200Oe$ ).

Due to the complexity and timing duration of the project, measurements on constructed devices have not been undertaken. Experiments on the sample should be performed in the future to clarify the copper oxidation state influence on its SOI properties. If successful, an identical experiment with insulating TmIG instead of TbCo could be performed in order to quantify the copper layer oxidation through a resistance measurement, as in this case Cu would be insulated in both boundaries. In this scenario, extracting the magnetisation state with low SMR signal instead of AHE would be an obstacle to overcome.

---

## 6 List of abbreviations

<b>AHE</b>	anomalous Hall effect.
<b>DL</b>	damping-like.
<b>FL</b>	field-like.
<b>FM</b>	ferromagnet.
<b>GGG</b>	gadolinium gallium garnet.
<b>HM</b>	heavy metals.
<b>IP</b>	in plane.
<b>MOKE</b>	magneto-optic Kerr effect.
<b>OOP</b>	out of plane.
<b>PMA</b>	perpendicular magnetic anisotropy.
<b>SHE</b>	spin Hall effect.
<b>SMR</b>	spin Hall magnetoresistance.
<b>SOI</b>	spin-orbit interaction.
<b>SOT</b>	spin-orbit torque.
<b>STT</b>	spin transfer torque.
<b>TmIG</b>	thulium iron garnet.

---

## 7 References

- [1] Arne Brataas, Andrew D. Kent, and Hideo Ohno. “Current-induced torques in magnetic materials”. In: *Nature Materials* 11.5 (2012), pp. 372–381. DOI: [10.1038/nmat3311](https://doi.org/10.1038/nmat3311).
- [2] Nicola A Spaldin. *Magnetic materials*. University Press, 2003.
- [3] Hongyu An et al. “Spin-torque generator engineered by natural oxidation of Cu”. In: *Nature Communications* 7.1 (2016). DOI: [10.1038/ncomms13069](https://doi.org/10.1038/ncomms13069).
- [4] Shilei Ding et al. “Harnessing Orbital-to-Spin Conversion of Interfacial Orbital Currents for Efficient Spin-Orbit Torques”. In: *Physical Review Letters* 125.17 (2020). DOI: [10.1103/physrevlett.125.177201](https://doi.org/10.1103/physrevlett.125.177201).
- [5] Can Onur Avci et al. *Fast switching and signature of efficient domain wall motion driven by spin-orbit torques in a perpendicular anisotropy magnetic insulator/Pt bilayer*. 2022.
- [6] Can Onur Avci et al. “Current-induced switching in a magnetic insulator”. In: *Nature Materials* 16.3 (2016), pp. 309–314. DOI: [10.1038/nmat4812](https://doi.org/10.1038/nmat4812).
- [7] Can Onur Avci. “Current-induced effects in ferromagnetic heterostructures due to spin-orbit coupling”. PhD thesis. ETH ZURICH, 2015.
- [8] Kannan Krishnan. *Fundamentals and Applications of Magnetic Materials*. Aug. 2016. ISBN: 9780199570447. DOI: [10.1093/acprof:oso/9780199570447.001.0001](https://doi.org/10.1093/acprof:oso/9780199570447.001.0001).
- [9] Jairo Sinova et al. “Universal Intrinsic Spin Hall Effect”. In: *Physical Review Letters* 92.12 (2004). DOI: [10.1103/physrevlett.92.126603](https://doi.org/10.1103/physrevlett.92.126603).
- [10] H. Kurebayashi et al. “An antidamping spin-orbit torque originating from the Berry curvature”. In: *Nature Nanotechnology* 9.3 (2014), pp. 211–217. DOI: [10.1038/nnano.2014.15](https://doi.org/10.1038/nnano.2014.15).
- [11] Dongwook Go et al. “Intrinsic Spin and Orbital Hall Effects from Orbital Texture”. In: *Physical Review Letters* 121.8 (2018). DOI: [10.1103/physrevlett.121.086602](https://doi.org/10.1103/physrevlett.121.086602).
- [12] A. Manchon et al. “Current-induced spin-orbit torques in ferromagnetic and antiferromagnetic systems”. In: *Reviews of Modern Physics* 91.3 (2019). DOI: [10.1103/revmodphys.91.035004](https://doi.org/10.1103/revmodphys.91.035004).
- [13] Kohei Ueda et al. “Spin-orbit torques in TA/TBXCo100-x ferrimagnetic alloy films with Bulk Perpendicular magnetic anisotropy”. In: *Applied Physics Letters* 109.23 (2016), p. 232403. DOI: [10.1063/1.4971393](https://doi.org/10.1063/1.4971393).
- [14] Uwe Bauer et al. “Magneto-ionic control of interfacial magnetism”. In: *Nature Materials* 14.2 (2014), pp. 174–181. DOI: [10.1038/nmat4134](https://doi.org/10.1038/nmat4134).

---

$$R_H^{SMR} = 22.655 m\Omega \quad H_{DL}/J_c = 7.5224 \cdot 10^{-12} \quad Oe \, m^2 \, A^{-1}$$